Materials Science & Engineering C 99 (2019) 1502–1508

Contents lists available at ScienceDirect

Materials Science & Engineering C

journal homepage: www.elsevier.com/locate/msec

Screen-printed interdigitated electrodes modified with nanostructured carbon nano-onion films for detecting the cancer biomarker CA19-9

Gisela Ibáñez-Redín[a,1], Roberto H.M. Furuta[a,1], Deivy Wilson[a], Flavio M. Shimizu[a,b], Elsa M. Materon[a,c], Lidia Maria Rebolho Batista Arantes[d], Matias E. Melendez[d], André L. Carvalho[d], Rui Manuel Reis[d,e,f], Manuel N. Chaur[g], Débora Gonçalves[a], Osvaldo N. Oliveira Jr[a,*]

[a] São Carlos Institute of Physics, University of São Paulo, 13560-970, São Carlos, SP, Brazil
[b] Brazilian Nanotechnology National Laboratory (LNNano), Brazilian Center for Research in Energy and Materials (CNPEM), 13083-970, Campinas, SP, Brazil
[c] Department of Chemistry, Federal University of São Carlos, 13565-970, São Carlos, SP, Brazil
[d] Molecular Oncology Research Center, Barretos Cancer Hospital, 14784-400, Barretos, SP, Brazil
[e] Life and Health Sciences Research Institute (ICVS), Health Sciences School, University of Minho, Braga, Portugal
[f] ICVS/3B's-PT Government Associate Laboratory, Braga/Guimarães, Portugal
[g] Departamento de Química, Universidad del Valle, Cl. 13 #100-00, Cali, Colombia

ARTICLE INFO

Keywords:
Screen-printed electrodes
Capacitive biosensors
Low-cost sensors
Carbon nano-onions
CA19-9
information visualization

ABSTRACT

Nanostructured capacitive biosensors, combined with inexpensive fabrication technologies, may provide simple, sensitive devices for detecting clinically relevant cancer biomarkers. Herein, we report a novel platform for detecting the pancreatic cancer biomarker CA19-9 using low-cost screen-printed interdigitated electrodes (SPIDEs). The SPIDEs were modified by carbon nano-onions (CNOs) and graphene oxide (GO) films, on which a layer of anti-CA19-9 antibodies was immobilized. The modification with CNOs and GO significantly improved the analytical performance of the biosensor, which displayed superior results to those prepared only with GO. The biossensor exhibited high reproducibility and a relatively low limit of detection of 0.12 U mL^{-1}. Using these devices in combination with information visualization methods we were able to detect CA19-9 in whole cell lysates of colorectal adenocarcinoma. The fabrication of these low-cost, disposable immunosensors is a successful attempt to explore CNOs in capacitive biosensors, which may be extended for detection of different cancer biomarkers.

1. Introduction

There is an increasing demand for detection and quantification of cancer biomarkers using analytical methods with accuracy and selectivity, with great promise for diagnosis, risk assessment, screening, prognosis, and monitoring of diseases. Current methods for detecting biomarkers, such as enzyme-linked immunosorbent assay (ELISA) and liquid chromatography-mass spectroscopy (LC-MS), are time-consuming and technically complex, and then incompatible with point-of-care routine testing [1]. Research efforts have been made toward faster and simpler technologies for sensing, which include capacitive biosensors based on interdigitated electrodes. Capacitive biosensors have been used to detect cancer biomarkers owing to their versatility, capability of miniaturization and ability to detect analytes without markers or redox probes [2–4]. They are usually prepared using photolithography techniques [5] to yield nanoscaled devices with high reproducibility; however, these preparation methodologies require clean environments, sophisticated instruments, several fabrication steps, and are time-consuming and costly [6,7]. Alternative technologies are now used to provide simple, inexpensive and accurate fabrication procedures [8–12], including screen-printing techniques that may allow for mass production of reproducible, low-cost devices with different sizes and shapes [13]. Furthermore, with screen printing one can also perform low-temperature deposition of conductive films on flexible substrates, such as paper [14,15] and polymers [16]. This is important for producing disposable biosensors for clinically relevant analytes, including bacteria [17], ammonia in the blood [18], cancer cells [11] and protein biomarkers [19].

* Corresponding author.
E-mail address: chu@ifsc.usp.br (O.N. Oliveira Jr).
[1] Gisela Ibáñez-Redín and Roberto H. M. Furuta contributed equally to this work.

https://doi.org/10.1016/j.msec.2019.02.065
Received 28 September 2018; Received in revised form 1 February 2019; Accepted 16 February 2019
Available online 19 February 2019
0928-4931/ © 2019 Elsevier B.V. All rights reserved.

In addition to being inexpensive and operationally simple, an ideal device for cancer biomarkers must have outstanding analytical features to enable detection of analytes at low concentrations. The incorporation of nanomaterials at the electrode surface has been explored to enhance sensitivity, as is the case of carbon nanotubes (CNTs) [20] and nanoparticles [21,22]. Carbon nano-onions (CNO) are carbon allotropes that consist of a concentric multilayered fullerene structure, remain relatively unexplored for sensing despite their interesting properties of high surface area, biocompatibility and electrical conductivity [23,24]. CNOs have been rather exploited in supercapacitors electrodes [25–28], but recently their potential for biosensors with electrochemical [29,30] and electrochemiluminescent transducers [31] was demonstrated. To the best of our knowledge, CNOs have not been used in capacitive immunosensors for detecting cancer biomarkers.

Pancreatic cancer is one of the most aggressive types with dismal prognosis [32]. At present, the carbohydrate antigen 19-9 (CA19-9), a high-molecular-weight glycoprotein [33], is one of the biomarkers for its early detection, but the methodologies used have low sensitivity. Here, we focused on the preparation of homemade Ag screen-printed interdigitated electrodes (SPIDEs) modified with CNOs and graphene oxide (GO) films for developing biosensors to detect CA19-9. This biomarker was chosen here to permit a straightforward comparison of low-cost electrodes and similar systems produced by our own group [4,34,35]. The cost per device unit of the novel SPIDEs produced here is ~ US$0.05, and they were entirely manufactured over polyethylene terephthalate (PET) and used as a low-cost alternative to commonly used Au electrodes. We verified that the modification with CNOs improves the analytical performance of immunosensors whose principle of detection is electrical impedance spectroscopy (EIS).

2. Materials and methods

2.1. Synthesis of CNOs and GO

CNOs were obtained by annealing ultradispersed nanodiamond particles (ND) (5 nm size) under an inert atmosphere at 1650 °C as previously described [36,61]. GO was synthesized using a modified Hummers' method [37,38], in which graphite powder was dispersed in a concentrated acidic mixture (H_2SO_4/H_3PO_4) and stirred during 2 h. Then, $KMnO_4$ was slowly added to the acidic mixture kept under magnetic agitation for 12 h using an oil bath, following the addition of an aqueous solution containing 10% H_2O_2. The final mixture was then centrifuged (4000 rpm for 0.5 h) to obtain a GO suspension in water.

2.2. Electrodes fabrication

The procedure for SPIDEs fabrication is schematically depicted in Fig. S1. The interdigitated arrays, *i.e.* 10 pairs of interdigitated electrodes, were designed using AutoCAD® (Autodesk, USA) and transferred to a 150 mesh polyester coated with a photo-emulsion printing screen [39]. The array patterns were printed on acetate sheets using a conventional laser printer (HP, USA), and then placed over the photo emulsion-coated screen. After exposure to UV light during 7 min, the soft emulsion was washed out, thus leaving shaped mold blanks. A single layer of Ag ink (PE410, DuPont, USA) was screen-printed over the polyethylene terephthalate (PET) sheets (35 × 24 cm^2) by using a semi-automatic printer (IMAH, Brazil) and following a thermal cure at 120 °C for 30 min. With this methodology, 200 electrodes can be produced in a single printing procedure.

2.3. Preparation of CNO-containing immunosensor for CA19-9

The fabrication procedure of the immunosensor is shown in Scheme 1. The SPIDEs were modified by depositing a fixed volume of 12 μL of CNOs/polyethyleneimine (PEI) dispersion (0.2 mg CNOs dispersed in 1 mL of 0.2 mg mL^{-1} of PEI aqueous solution). The electrodes were dried for 2 h, followed by adsorption of 6 μL of GO in an aqueous solution at 0.5 mg mL^{-1}. A fixed volume of 6 μL of CA19-9 antibody (Ab) (Aviva Systems Biology, USA) in phosphate buffer (1:5 vol./vol. ratio) was left for 3 h over the electrode surface for spontaneous adsorption. The modified electrode was then washed with 0.1 mol L^{-1} phosphate buffer (pH 7.0) to remove weakly adsorbed antibodies. Finally, the biosensor obtained, SPIDE/CNO-GO-Ab, was washed with phosphate buffer. For comparison purposes, a biosensor without CNOs (SPIDE/GO-Ab) was also fabricated following the same procedure described.

2.4. Electrical measurements

The impedance spectroscopy measurements were conducted using a Solartron 1260A with an applied potential of 50 mV. The capacitance values were measured in a frequency range from 1 Hz to 10^6 Hz using SMaRT Impedance Measurement Software. The analytical curves were constructed from the measurements obtained after depositing 10 μL of different concentrations of human pancreatic cancer antigen CA19-9 (Aviva System Biology, USA) over the biosensors allowing it to react during an optimized time of 10 min. Then, they were washed, and the measurements were performed using 30 μL of phosphate buffer at 0.1 mol L^{-1} (pH 7.0). The selectivity and applicability of the biosensors were assessed with regard to possible interferences, *e.g.* from p16 antigen and vimentin biomarkers. Their analytical responses were also evaluated by using whole cell lysates of colorectal adenocarcinoma from HT-29 (CA19-9 expressing) and SW-620 (CA19-9 null) cell lines, which were lysed by three cycles of freeze–thaw and stored at −80 °C following a procedure described elsewhere [4]. The cell lysates were preserved in a solution containing 10% fetal bovine serum (FBS), 2.0 mmol L^{-1} glutamine, 1% penicillin/streptomycin, and kept in a CO_2 incubator at 37 °C. Then, they were washed with phosphate-buffered saline (PBS) solution, and after 48 h of incubation, the supernatants were obtained by filtration, and were stored at −80 °C prior to being finally analyzed [4]. Cell line authentication was carried out by the Center for Molecular Diagnostics of Barretos Cancer Hospital (São Paulo, Brazil) as previously reported [40].

2.5. Characterization

The film thickness was determined using a Dektak XT profilometer (Bruker Corp.). Scanning electron microscope (SEM) images were obtained using a ZEISS Sigma microscopy. High Resolution Transmission Electron Microscope (HRTEM) images were obtained using a Tecnai G2 F20 (FEI) microscopy, and atomic force microscope (AFM) experiments were performed using a Bruker dimension FastScan.

2.6. Data analysis

The capacitance was measured in a frequency range of 1 Hz to 1 MHz and diverse analyte concentrations, thus generating considerable amounts of data. One way to mine such data is through multidimensional projection techniques combined with information visualization methods [41]. Here we tested the following projection techniques to analyze the data: Principal Component Analysis (PCA) [42], Partial Least Square (PLS) [43], nonlinear Sammon's mapping [44] and IDMAP (Interactive Document Map) [45], implemented in the software PEx-Sensors [41]. Capacitance data were normalized and dimensionally reduced by linear PCA and nonlinear *Fastmap* [46] techniques and dissimilarity between samples were converted to Euclidean distances as the metric for projection. The distinguishing ability was quantified using the silhouette coefficient, *S*, whose values close to 1 mean that the curves are distinct from each other, while values close to 0 mean that the measurement does not assist in distinguishing the samples [47].

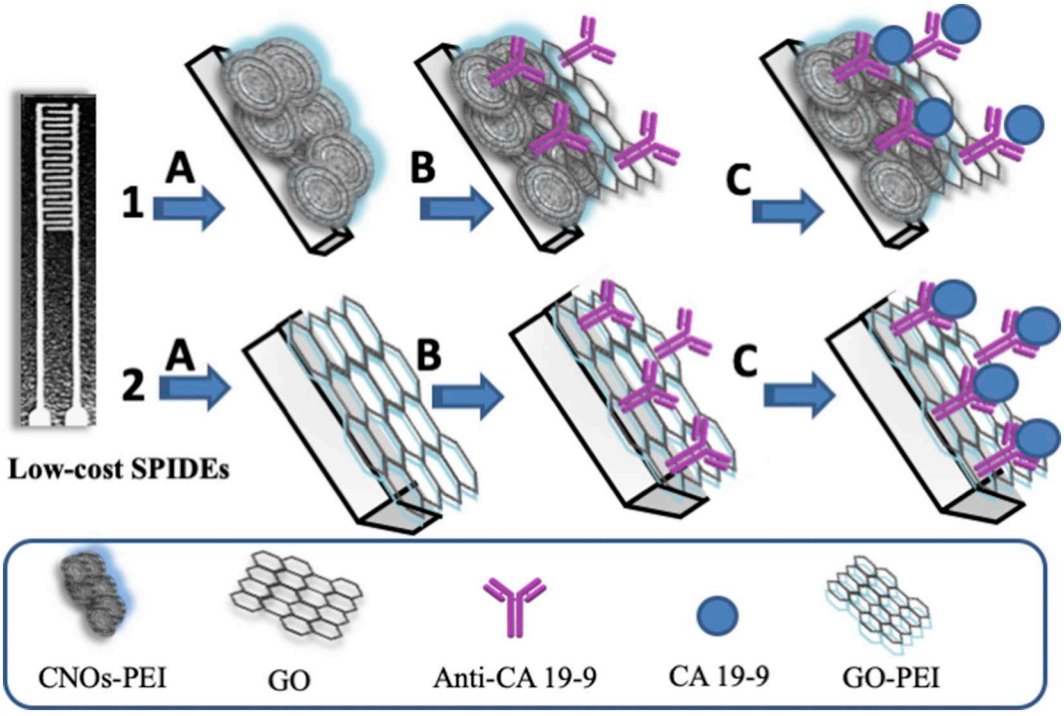

Scheme 1. Illustration for biosensors fabrication (SPIDE/CNO-GO-Ab (1) and SPIDE/GO-Ab (2)) and CA19-9 detection process. The overall process involves: electrode modification (A), antibody immobilization (B) and CA19-9 incubation (C).

3. Results and discussion

Low-cost, screen-printing protocols were used for large-scale production of flexible, disposable SPIDEs based on Ag layers separated by 180 μm width. The cost of the materials used per device unit is ~ US $0.05. Fig. 1(A, B) show the electrodes built with an 8.5 μm thick Ag layer on a PET substrate. The electrode surface has a heterogeneous morphology according to the scanning electron microscopy (SEM) image in Fig. 1(C), which is rich in Ag flakes. The electrical response of SPIDEs as a function of the electrolyte conductivity was also investigated, with the devices being capable of distinguishing between different concentrations of NaCl solutions from 0.001 to 1 mol L^{-1} (Fig. 1(D)). The increment in the ionic concentration leads to a change in the surface dielectric properties, which are reflected in a capacitance

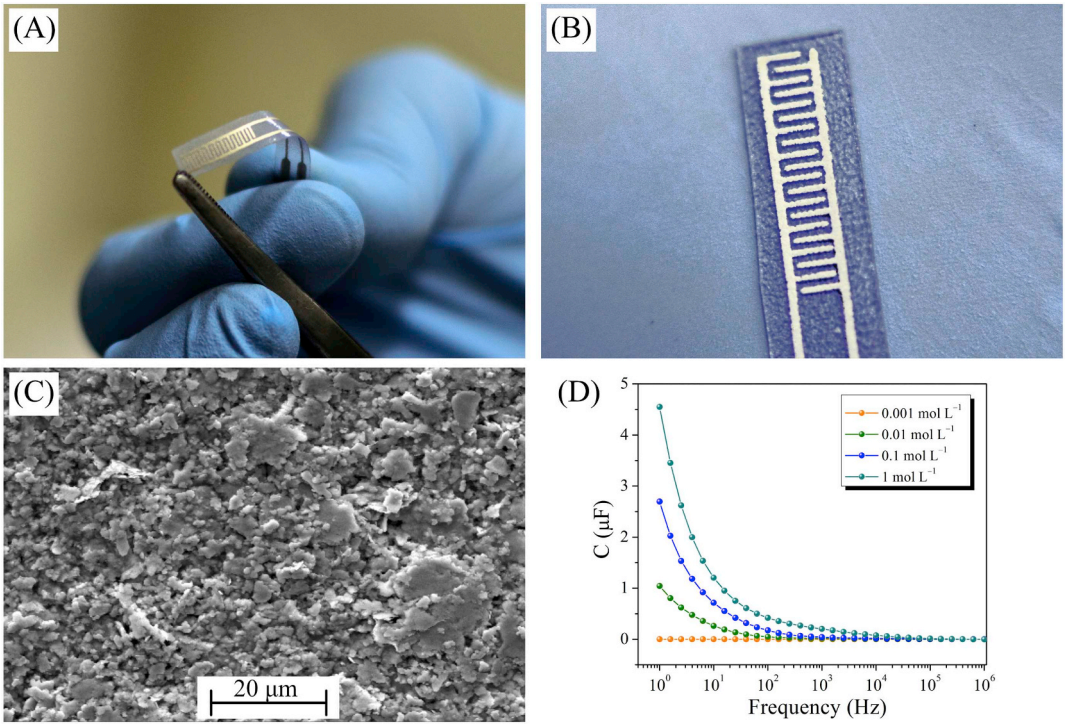

Fig. 1. Picture of SPIDEs (A,B), SEM image of bare SPIDE (C) and capacitance spectra of bare SPIDE obtained using NaCl solutions from 1.0×10^{-3} mol L^{-1} to 1.0 mol L^{-1} (D).

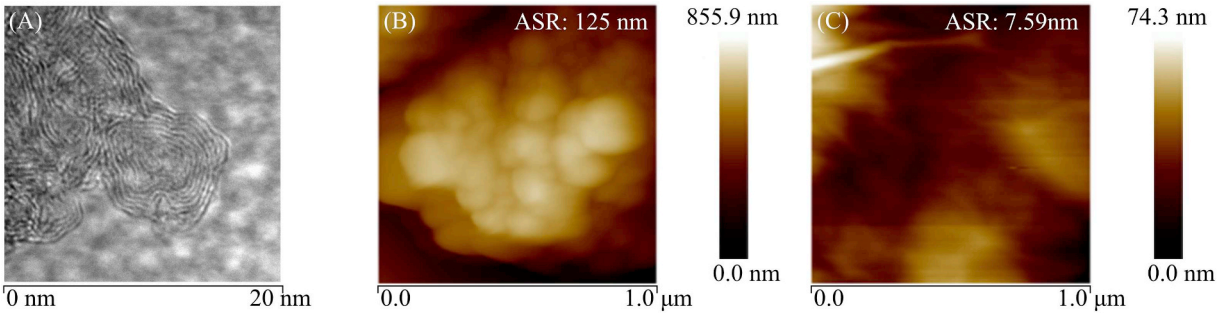

Fig. 2. HRTEM image of CNOs (A) and AFM images of: SPIDE/CNO-GO-Ab (B) and SPIDE/GO-Ab (C).

increase for frequencies below 10^4 Hz. At the upper frequency region the electrical response is mainly dominated by the electrode geometry [48] with a negligible impact of the solution conductivity.

The sensor platform (SPIDE/CNO-GO) was fabricated by first depositing, *via* drop casting, a layer of CNOs whose diameter was 10 nm as determined by TEM (Fig. 2(A)). Due to the low dispersibility of CNOs in water, a cationic polyelectrolyte (PEI) in an aqueous solution was used as the dispersion medium in order to improve mechanical stability of the modified electrodes [49,50]. A negatively-charged top layer of GO was subsequently adsorbed on the electrode surface which allowed immobilization by electrostatic interaction of a layer of antibodies. Capacitance measurements were conducted to characterize the assembly process of the biosensor (see Fig. S2(A, B), in the Supporting Information). The high surface area and mesoporous nature of CNOs leads to porous films with large roughness [49] as confirmed in the AFM analysis (Fig. 2(B, C)), which reveals a 16-fold increase of the SPIDE/CNO-GO surface roughness compared to the electrodes without incorporation of CNOs (SPIDE/GO). Such an increase in electrode/electrolyte contact surface leads to a higher electrical capacitance in Fig. S2(B), also improving the analytical performance of the immunosensor.

The CA19-9 antigen pancreatic biomarker diluted in phosphate buffer solution was detected with capacitance measurements on SPIDE/GO-Ab and SPIDE/CNO-GO-Ab architectures. Fig. 3(A,B) shows capacitance *vs* frequency plots, from which one notes that the capacitance decreases with increasing CA19-9 concentration at low frequencies. This behavior can be attributed to the antigen adsorption displacing out the ions and water molecules from the surface [51]. Fig. 3(C) shows the analytical curves at 1 Hz, a frequency in which electric double-layer effects are important. The curves were obtained for concentrations ranging from 0.3 to 70 U mL^{-1} and 0.3 to 100 U mL^{-1} for SPIDE/GO-Ab and SPIDE/CNO-GO-Ab, respectively, according to the following regression equations:

$$\text{SPIDE/GO} - \text{Ab: (C blank–C)}\ (\mu\text{F}) = (0.24 \pm 0.02) + (0.23 \pm 0.02)\log[\text{CA 19–9}]\ (\text{U mL}^{-1}),\quad r = 0.9451$$

$$\text{SPIDE/CNO} - \text{GO} - \text{Ab: (C blank–C)}\ (\mu\text{F}) = (0.36 \pm 0.02) + (0.50 \pm 0.02)\log[\text{CA 19–9}]\ (\text{U mL}^{-1}),\quad r = 0.9940$$

The immunosensor with SPIDE/CNO-GO-Ab architecture exhibited a higher sensitivity (0.50 μF log[CA19-9]$^{-1}$) than SPIDE/GO-Ab (0.23 μF log[CA19-9]$^{-1}$). The limit of detection (LD) was calculated as three times the standard deviation of the analytical curve intercept divided by the slope [52], leading to 0.26 and 0.12 U mL^{-1} for SPIDE/GO-Ab and SPIDE/CNO-GO-Ab, respectively. Both platforms exhibited analytical parameters comparable to those reported in the literature [4,34,35,53,54], including capacitive biosensors fabricated with gold interdigitated electrodes, as observed in Table 1. Since the SPIDE/CNO-GO-Ab immunosensor presented the best performance for CA19-9 detection, further experiments and analyses were focused only on this architecture.

The changes induced by CA19-9 can be better expressed in terms of relative capacitance (difference between the capacitance response with and without antigen). Fig. S3(A) shows the pronounced effect attributed to changes in the double-layer region that governs the electrical response at low frequencies. The concentration dependence is visualized in Fig. S3(B), whose data may be explained with the Langmuir-Freundlich model isotherm [55,56] represented in Eq. (1):

$$q = \frac{Q_m (KC_{sat})^n}{(KC_{sat})^n + 1} \quad (1)$$

where q is the amount of adsorbed antigen on biosensor surface, and C_{sat} is the solution concentration at equilibrium. Upon fitting with this model, we determined the values of adsorption capacity (C_{sat}), affinity

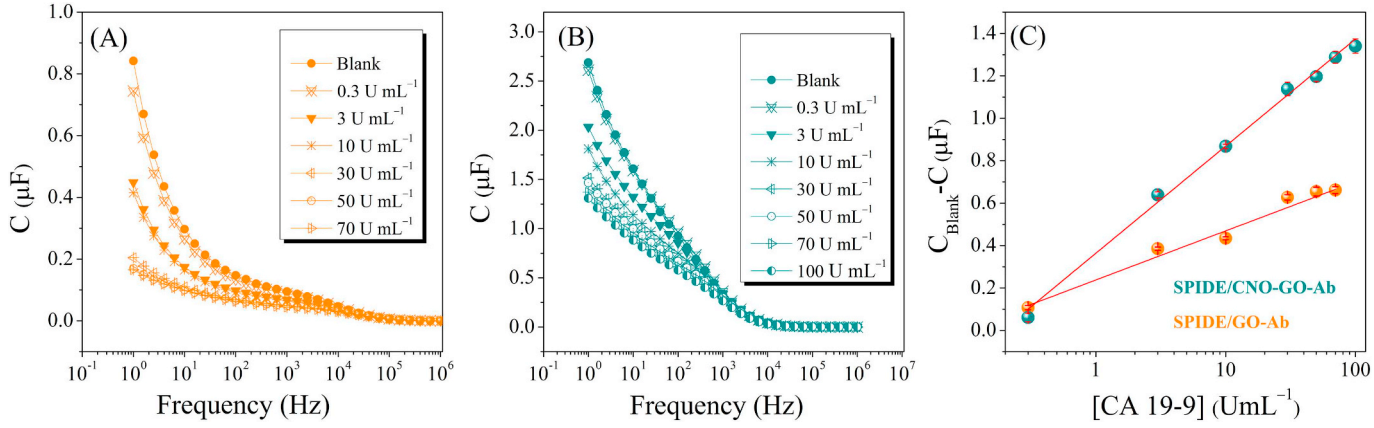

Fig. 3. Capacitance *vs* frequency spectra obtained for different concentrations of CA19-9 on SPIDE/GO-Ab (A) and SPIDE/CNO-GO-Ab (B). Calibration curves (C).

Table 1
Comparison of analytical parameters obtained for CA19-9 determination using SPIDE/GO-Ab and SPIDE/CNO-GO-Ab with results from the literature.

Electrode	Technique	LD (U mL^{-1})	Concentration range (U mL^{-1})	Reference
PEI-CNT	EIS	0.30	0.05-60	[4]
chitosan/ Con A	EIS	0.69	4-100	[34]
11-MUA/EDC/NHS/anti- CA19-9	EIS	0.68	0.1-189	[35]
PPPD-Au/Pt GCE	DPV	2.3×10^{-4}	0.001-40	[53]
BSA/anti-CA19-9/AuPtNCs/GCE	DPV	0.03	0.05-50	[54]
SPIDE/GO-Ab	EIS	0.26	0.3-70	This work
SPIDE/CNO-GO-Ab	EIS	0.12	0.3-100	

PEI: polyethyleneimine; CNT: Carbon nanotubes; EIS: electrical impedance spectroscopy; Con A: concavalin A; 11-MUA: 11-Mercaptoundecanoic acid; EDC: 1-Ethyl-3-(3-dimethylaminopropyl) carbodiimide; NHS: N-Hydroxysuccinimide; PPPD: poly(-N,N-diphenyl-p-phenylediamine); GCE: glassy carbon electrode; DPV: differential pulse voltammetry; BSA: bovine serum albumin; NCs: AuPt nanocalliandras.

constant for adsorption (K) and index of heterogeneity (n). The saturation of the available sites occurs at $C_{sat} = -2.18\,\mu F$, which corresponds to $\sim 280\,U\,mL^{-1}$. The affinity constant for adsorption is 0.61, higher than the value found in the literature [35] probably owing to effects of surface heterogeneity with $n = 0.46$.

When considerable amounts of data are available, as with impedance spectra, distinguishing similar samples may be more effective if a feature selection procedure is performed in the data analysis. For spectra, in particular, one may select the frequencies at which the response provides the best distinguishing ability. Fig. 4 shows the capacitance data plotted using the parallel coordinates technique [57], with which we determined the dimensions (frequencies) that contribute most to detection (blue boxes) and those that did not (red boxes). From 31 dimensions only 2 presented red boxes at high frequencies. Even though only two frequencies had to be eliminated, feature selection still provided positive results, as will be demonstrated with Fig. 5.

The capacitance data were also plotted using four multidimensional projection techniques, *viz.* IDMAP, Sammon's mapping, PCA and PLS, all of which were adequate for distinguishing the various concentrations of CA19-9. Based on the silhouette coefficients, IDMAP and PCA provided the best performance with S = 0.94 after feature selection, as indicated in Fig. 5.

The ability to distinguish the samples is illustrated in the IDMAP plot of Fig. 6(A), where each capacitance spectrum is represented by a graphical marker in a set of three independent measurements. IDMAP was chosen because it has been proven effective for treating biosensing

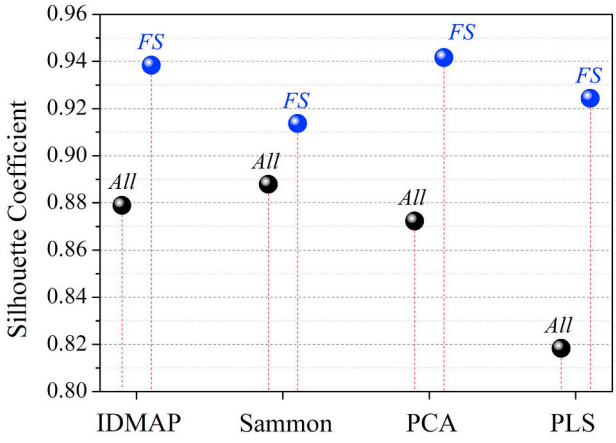

Fig. 5. Silhouette coefficient values for projection techniques IDMAP, Sammon's mapping, PCA, PLS treated (FS) and non-treated (All) with feature selection method.

data in several cases [4,58]. One can note the lowest concentration used, $0.3\,U\,mL^{-1}$, is considerably distant from the phosphate buffer samples, which is consistent with the calculated LD = $0.12\,U\,mL^{-1}$. This low LD and wide concentration range for distinction in the plot are important for determining the biomarker in real samples, since the threshold value to consider a patient with pancreatic cancer is

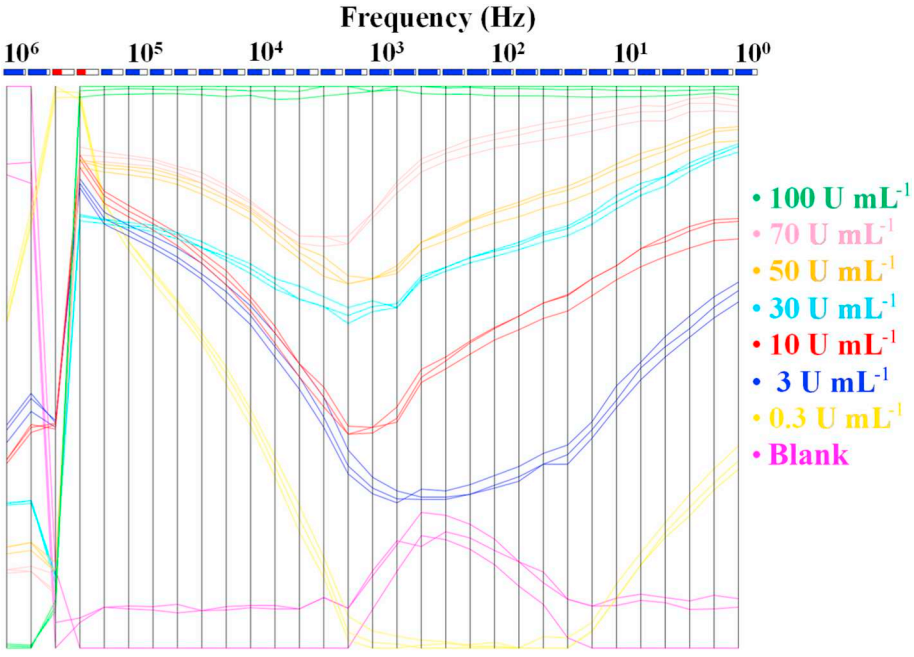

Fig. 4. Parallel coordinates plot for the capacitance data measured with SPIDE/CNO-GO-Ab electrodes at different CA19-9 concentrations. A larger number of blue boxes are seen, which means that most frequencies are suitable for distinguishing among the samples. (For interpretation of the references to colour in this figure legend, the reader is referred to the web version of this article.)

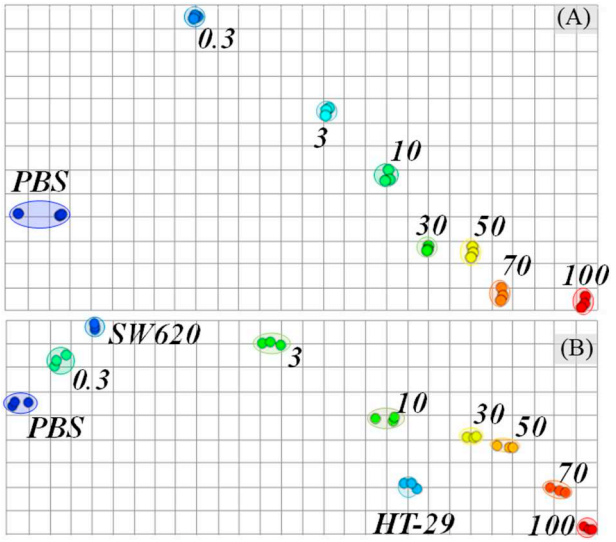

Fig. 6. IDMAP plot with feature selection treatment for capacitance *vs.* frequency data of CA19-9 commercial samples at concentrations from 0.3 U mL^{-1} to 100 U mL^{-1} (A). IDMAP plot with feature selection for capacitance *vs.* frequency data of CA19-9 commercial samples from 0.3 U mL^{-1} to 100 U mL^{-1} and real HT29 and SW620 samples (B).

37 U mL^{-1}. It should be stressed that measuring CA19-9 concentration at different levels has clinical relevance because one may predict disease remission, survival, tumor stage, patient response to chemotherapy or even predict recurrence and metastases. For example, high levels of CA19-9 (< 68.8 U mL^{-1}) are associated with surgical resectability, which might be a tool for making decision about the best treatment. On the other hand, diseases such as chronic fibrosing pancreatitis have lower thresholds (< 37 U mL^{-1}) [59,60].

The data for the commercial samples are plotted in Fig. 6(B), alongside the samples from cell lines lysates that were tested positive (HT29) and negative (SW620) for the biomarker CA19-9. It is significant that the data points for these real samples are located as expected in the plot, with the HT29 sample - which contains 12.3 U mL^{-1} of CA19-9 - being placed between commercial samples with 10 and 30 U mL^{-1}. Furthermore, the sample for the cell line SW620 appears very close to phosphate buffer and 0.3 U mL^{-1} data points, as expected.

To confirm the immunosensor selectivity, control experiments were carried out with two possible interferents (p16 and vimentin). No significant change was observed in the capacitance spectra, as shown in Fig. S4(A) in the Supporting Information. We also compared the response of SPIDE/CNO-GO-Ab with that of a platform without immobilized antibody (SPIDE/CNO-GO) at different CA19-9 concentrations. Fig. S4(B) shows the changes in the capacitance spectra in the absence of immobilized antibody, which are considerably lower than those seen for the SPIDE/CNO-GO-Ab biosensor. This confirms that such differences in electrical response are mainly promoted by antigen-antibody interactions. The immunosensor also displayed excellent inter-day fabrication reproducibility with relative standard deviation (RSD) of 8.11% (see Fig. S4(C)).

4. Conclusions

We developed a capacitive immunosensor for detecting the cancer biomarker CA19-9 using low-cost screen-printed interdigitated electrodes (SPIDEs) modified with CNOs and GO films. The fabrication protocol allowed the production of hundreds of SPIDEs in a few minutes, using simple and inexpensive materials. Modification with nanostructured CNOs and GO films improved the analytical properties of the device, providing a reproducible and simple platform which can detect CA19-9 with a limit of detection of 0.12 U mL^{-1}. The immunosensor also displayed a wide dynamic range (from 0.3 to 100 U mL^{-1}), within the clinically relevant range for detection of different disorders, including pancreatic cancer. Assays with other proteins to verify selectivity have supported the specificity of the biosensor toward CA19-9. Using multidimensional projection techniques implemented in the PEx-Sensors software, we were able to discriminate with 100% accuracy all the samples containing CA19-9. This sensor platform is generic, and may be explored for other biosensors, being amenable for point-of-care diagnosis. In addition, since the immunosensor was fabricated on flexible substrates, it can be applied as a non-invasive sensor, biointegrated onto the skin to be able to use sweat, saliva or urine as samples.

Acknowledgements

This work was supported by CAPES (001), CNPq, INEO and FAPESP (2012/15543-7, 2013/14262-7, 2015/01770-0, 2016/00991-5 and 2017/12096-3). M.N.C is grateful for the economic support from Vicerrectoria de Investigaciones and the Centro de Excelencia en Nuevos Materiales (CENM) from the Universidad del Valle.

Appendix A. Supplementary data

Supplementary data to this article can be found online at https://doi.org/10.1016/j.msec.2019.02.065.

References

[1] J.F. Rusling, C.V. Kumar, J.S. Gutkind, V. Patel, Measurement of biomarker proteins for point-of-care early detection and monitoring of cancer, Analyst 135 (2010) 2496–2511.
[2] S.K. Arya, P. Zhurauski, P. Jolly, M.R. Batistuti, M. Mulato, P. Estrela, Capacitive aptasensor based on interdigitated electrode for breast cancer detection in undiluted human serum, Biosens. Bioelectron. 102 (2018) 106–112.
[3] P. Zhurauski, S.K. Arya, P. Jolly, C. Tiede, D.C. Tomlinson, P. Ko Ferrigno, et al., Sensitive and selective Affimer-functionalised interdigitated electrode-based capacitive biosensor for Her4 protein tumour biomarker detection, Biosens. Bioelectron. 108 (2018) 1–8.
[4] A. Thapa, A.C. Soares, J.C. Soares, I.T. Awan, D. Volpati, M.E. Melendez, et al., Carbon nanotube matrix for highly sensitive biosensors to detect pancreatic cancer biomarker CA19-9, ACS Appl. Mater. Interfaces 9 (2017) 25878–25886.
[5] V. Tsouti, C. Boutopoulos, I. Zergioti, S. Chatzandroulis, Capacitive microsystems for biological sensing, Biosens. Bioelectron. 27 (2011) 1–11.
[6] C.K. Tang, A. Vaze, J.F. Rusling, Fabrication of immunosensor microwell arrays from gold compact discs for detection of cancer biomarker proteins, Lab Chip 12 (2012) 281–286.
[7] A.J. Killard, Disposable sensors, Current Opinion in Electrochemistry 3 (2017) 57–62.
[8] S. Carvajal, S.N. Fera, A.L. Jones, T.A. Baldo, I.M. Mosa, J.F. Rusling, et al., Disposable inkjet-printed electrochemical platform for detection of clinically relevant HER-2 breast cancer biomarker, Biosens. Bioelectron. 104 (2018) 158–162.
[9] F.J. Pavinatto, C.W.A. Paschoal, A.C. Arias, Printed and flexible biosensor for antioxidants using interdigitated ink-jetted electrodes and gravure-deposited active layer, Biosens. Bioelectron. 67 (2015) 553–559.
[10] T. Yang, Y.Z. Yu, L.S. Zhu, X. Wu, X.H. Wang, J. Zhang, Fabrication of silver interdigitated electrodes on polyimide films via surface modification and ion-exchange technique and its flexible humidity sensor application, Sens Actuat B Chem 208 (2015) 327–333.
[11] A.F.M. Mansor, I. Ibrahim, A.A. Zainuddin, I. Voiculescu, A.N. Nordin, Modeling and development of screen-printed impedance biosensor for cytotoxicity studies of lung carcinoma cells, Med Biol Eng Comput 56 (2018) 173–181.
[12] A.K. Assaifan, J.S. Lloyd, S. Samavat, D. Deganello, R.J. Stanton, K.S. Teng, Nanotextured surface on flexographic printed ZnO thin films for low-cost non-Faradaic biosensors, ACS Appl. Mater. Interfaces 8 (2016) 33802–33810.
[13] M. Trojanowicz, Impact of nanotechnology on design of advanced screen-printed electrodes for different analytical applications, TrAC Trends Anal. Chem. 84 (2016) 22–47.
[14] S. Cinti, D. Talarico, G. Palleschi, D. Moscone, F. Arduini, Novel reagentless paper-based screen-printed electrochemical sensor to detect phosphate, Anal. Chim. Acta 919 (2016) 78–84.
[15] P.J. Lamas-Ardisana, P. Casuso, I. Fernandez-Gauna, G. Martínez-Paredes, E. Jubete, L. Añorga, et al., Disposable electrochemical paper-based devices fully fabricated by screen-printing technique, Electrochem. Commun. 75 (2017) 25–28.
[16] L.R. Cumba, J.P. Smith, D.A. Brownson, J. Iniesta, J.P. Metters, D.R. do Carmo, et al., Electroanalytical detection of pindolol: comparison of unmodified and reduced graphene oxide modified screen-printed graphite electrodes, Analyst 140 (2015) 1543–1550.

[17] A.C. Ward, A.J. Hannah, S.L. Kendrick, N.P. Tucker, G. MacGregor, P. Connolly, Identification and characterisation of Staphylococcus aureus on low cost screen printed carbon electrodes using impedance spectroscopy, Biosens. Bioelectron. 110 (2018) 65–70.
[18] N.T. Brannelly, A.J. Killard, An electrochemical sensor device for measuring blood ammonia at the point of care, Talanta 167 (2017) 296–301.
[19] C. Fernández-Sánchez, C.J. McNeil, K. Rawson, O. Nilsson, Disposable non-competitive immunosensor for free and total prostate-specific antigen based on capacitance measurement, Anal. Chem. 76 (2004) 5649–5656.
[20] A. Qureshi, I. Roci, Y. Gurbuz, J.H. Niazi, An aptamer based competition assay for protein detection using CNT activated gold-interdigitated capacitor arrays, Biosens. Bioelectron. 34 (2012) 165–170.
[21] Z. Altintas, S.S. Kallempudi, U. Sezerman, Y. Gurbuz, A novel magnetic particle-modified electrochemical sensor for immunosensor applications, Sens Actuat B Chem 174 (2012) 187–194.
[22] H.W. Jung, Y.W. Chang, G.Y. Lee, S. Cho, M.J. Kang, J.C. Pyun, A capacitive biosensor based on an interdigitated electrode with nanoislands, Anal. Chim. Acta 844 (2014) 27–34.
[23] J. Luszczyn, M.E. Plonska-Brzezinska, A. Palkar, A.T. Dubis, A. Simionescu, D.T. Simionescu, et al., Small noncytotoxic carbon nano-onions: first covalent functionalization with biomolecules, Chemistry (Easton) 16 (2010) 4870–4880.
[24] O. Mykhailiv, H. Zubyk, M.E. Plonska-Brzezinska, Carbon nano-onions: Unique carbon nanostructures with fascinating properties and their potential applications, Inorg. Chim. Acta 468 (2017) 49–66.
[25] M.E. Plonska-Brzezinska, D.M. Brus, A. Molina-Ontoria, L. Echegoyen, Synthesis of carbon nano-onion and nickel hydroxide/oxide composites as supercapacitor electrodes, RSC Adv. 3 (2013) 25891–25901.
[26] Y. Gao, Y.S. Zhou, M. Qian, X.N. He, J. Redepenning, P. Goodman, et al., Chemical activation of carbon nano-onions for high-rate supercapacitor electrodes, Carbon 51 (2013) 52–58.
[27] D. Pech, M. Brunet, H. Durou, P. Huang, V. Mochalin, Y. Gogotsi, et al., Ultrahigh-power micrometre-sized supercapacitors based on onion-like carbon, Nat. Nanotechnol. 5 (2010) 651.
[28] M.E. Plonska-Brzezinska, L. Echegoyen, Carbon nano-onions for supercapacitor electrodes: recent developments and applications, J. Mater. Chem. A 1 (2013) 13703–13714.
[29] J.P. Bartolome, L. Echegoyen, A. Fragoso, Reactive carbon nano-onion modified glassy carbon surfaces as DNA sensors for human papillomavirus oncogene detection with enhanced sensitivity, Anal. Chem. 87 (2015) 6744–6751.
[30] J. Mohapatra, B. Ananthoju, V. Nair, A. Mitra, D. Bahadur, N.V. Medhekar, et al., Enzymatic and non-enzymatic electrochemical glucose sensor based on carbon nano-onions, Appl. Surf. Sci. 442 (2018) 332–341.
[31] M. Rizwan, N.F. Mohd-Naim, N.A. Keasberry, M.U. Ahmed, A highly sensitive and label-free electrochemiluminescence immunosensor for beta 2-microglobulin, Anal. Methods 9 (2017) 2570–2577.
[32] C.E. DeSantis, C.C. Lin, A.B. Mariotto, R.L. Siegel, K.D. Stein, J.L. Kramer, et al., Cancer treatment and survivorship statistics, CA Cancer J. Clin. 64 (2014) 252–271.
[33] K.S. Goonetilleke, A.K. Siriwardena, Systematic review of carbohydrate antigen (CA 19-9) as a biochemical marker in the diagnosis of pancreatic cancer, European Journal of Surgical Oncology (EJSO) 33 (2007) 266–270.
[34] A.C. Soares, J.C. Soares, F.M. Shimizu, M.E. Melendez, A.L. Carvalho, O.N. Oliveira, Controlled film architectures to detect a biomarker for pancreatic cancer using impedance spectroscopy, ACS Appl. Mater. Interfaces 7 (2015) 25930–25937.
[35] A.C. Soares, J.C. Soares, F.M. Shimizu, V.d.C. Rodrigues, I.T. Awan, M.E. Melendez, et al., A simple architecture with self-assembled monolayers to build immunosensors for detecting the pancreatic cancer biomarker CA19-9, Analyst 143 (2018) 3302–3308.
[36] J. Yang, Y. Zhang, D.Y. Kim, Electrochemical sensing performance of nanodiamond-derived carbon nano-onions: comparison with multiwalled carbon nanotubes, graphite nanoflakes, and glassy carbon, Carbon 98 (2016) 74–82.
[37] G. Ibáñez-Redín, D. Wilson, D. Gonçalves, O.N. Oliveira, Low-cost screen-printed electrodes based on electrochemically reduced graphene oxide-carbon black nanocomposites for dopamine, epinephrine and paracetamol detection, J. Colloid Interface Sci. 515 (2018) 101–108.
[38] W.S. Hummers, R.E. Offeman, Preparation of graphitic oxide, J. Am. Chem. Soc. 80 (1958) (1339–1339).
[39] G.W. Bishop, B.K. Ahiadu, J.L. Smith, J.D. Patterson, Use of redox probes for characterization of layer-by-layer gold nanoparticle-modified screen-printed carbon electrodes, J. Electrochem. Soc. 164 (2016) B23–B28 (B23-B8).
[40] R.J. Silva-Oliveira, V.A.O. Silva, O. Martinho, A. Cruvinel-Carloni, M.E. Melendez, M.N. Rosa, et al., Cytotoxicity of allitinib, an irreversible anti-EGFR agent, in a large panel of human cancer-derived cell lines: KRAS mutation status as a predictive biomarker, Cell. Oncol. 39 (2016) 253–263.
[41] F.V. Paulovich, M.L. Moraes, R.M. Maki, M. Ferreira, O.N. Oliveira, M.C.F. Oliveira, Information visualization techniques for sensing and biosensing, Analyst 136 (2011) 1344–1350.
[42] I.T. Jolliffe, Principal Component Analysis and Factor Analysis, Principal Component Analysis, Springer New York, New York, NY, 1986, pp. 115–128.
[43] G. Paul, Notes on the history and nature of partial least squares (PLS) modelling, J. Chemom. 2 (1988) 231–246.
[44] J.W. Sammon, A nonlinear mapping for data structure analysis, IEEE Trans Comput, C 18 (1969) 401–409.
[45] R. Minghim, F.V. Paulovich, A.A. Lopes, Content based text mapping using multi-dimensional projections for exploration of document collections, Proc. SPIE 6060 (2006) (60600S-1-60600S-12).
[46] C. Faloutsos, K.-I. Lin, FastMap: a fast algorithm for indexing, data-mining and visualization of traditional and multimedia datasets, SIGMOD Rec 24 (1995) 163–174.
[47] P.N. Tan, M. Steinbach, V. Kumar, Introduction to Data Mining: Pearson Addison Wesley, (2006).
[48] V.F. Lvovich, Impedance Spectroscopy: Applications to Electrochemical and Dielectric Phenomena, Wiley, 2012.
[49] J. Breczko, M.E. Plonska-Brzezinska, L. Echegoyen, Electrochemical oxidation and determination of dopamine in the presence of uric and ascorbic acids using a carbon nano-onion and poly(diallyldimethylammonium chloride) composite, Electrochim. Acta 72 (2012) 61–67.
[50] J. Breczko, K. Winkler, M.E. Plonska-Brzezinska, A. Villalta-Cerdas, L. Echegoyen, Electrochemical properties of composites containing small carbon nano-onions and solid polyelectrolytes, J. Mater. Chem. 20 (2010) 7761–7768.
[51] J.J. Davis, R.S.o. chemistry, Engineering the Bioelectronic Interface: Applications to Analyte Biosensing and Protein Detection, Royal Society of Chemistry, 2009.
[52] J.N. Miller, J.C. Miller, Statistics and Chemometrics for Analytical Chemistry, Pearson/Prentice Hall, 2005.
[53] L. Wang, J. Shan, F. Feng, Z. Ma, Novel redox species polyaniline derivative-Au/Pt as sensing platform for label-free electrochemical immunoassay of carbohydrate antigen 199, Anal. Chim. Acta 911 (2016) 108–113.
[54] X. Weng, Y. Liu, Y. Xue, A.-J. Wang, L. Wu, J.-J. Feng, L-Proline bio-inspired synthesis of AuPt nanocalliandras as sensing platform for label-free electrochemical immunoassay of carbohydrate antigen 19-9, Sens Actuat B Chem 250 (2017) 61–68.
[55] S. Liu, Cooperative adsorption on solid surfaces, J. Colloid Interface Sci. 450 (2015) 224–238.
[56] G.P. Jeppu, T.P. Clement, A modified Langmuir-Freundlich isotherm model for simulating pH-dependent adsorption effects, J. Contam. Hydrol. 129-130 (2012) 46–53.
[57] C.M. Daikuzono, F.M. Shimizu, A. Manzoli, A. Riul, M.H.O. Piazzetta, A.L. Gobbi, et al., Information visualization and feature selection methods applied to detect gliadin in gluten-containing foodstuff with a microfluidic electronic tongue, ACS Appl. Mater. Interfaces 9 (2017) 19646–19652.
[58] J.C. Soares, A.C. Soares, P.A. Pereira, V.C. Rodrigues, F.M. Shimizu, M.E. Melendez, et al., Adsorption according to the Langmuir-Freundlich model is the detection mechanism of the antigen p53 for early diagnosis of cancer, Phys. Chem. Chem. Phys. 18 (2016) 8412–8418.
[59] M.A. Tempero, E. Uchida, H. Takasaki, D.A. Burnett, Z. Steplewski, P.M. Pour, Relationship of carbohydrate antigen 19-9 and Lewis antigens in pancreatic cancer, Cancer Res. 47 (1987) 5501–5503.
[60] K.E. Poruk, D.Z. Gay, K. Brown, J.D. Mulvihill, K.M. Boucher, C.L. Scaife, et al., The clinical utility of CA 19-9 in pancreatic adenocarcinoma: diagnostic and prognostic updates, Curr. Mol. Med. 13 (2013) 340–351.
[61] L. Echegoyen, A. Ortiz, M.N. Chaur, A.J. Palkar, Carbon Nano Onions, in: T. Akasaka, F. Wudl, S. Nagase (Eds.), Chemistry of Nanocarbons, John Wiley & Sons, Chichester, U.K., 2010, pp. 463–483, , https://doi.org/10.1002/9780470660188.ch19.